Cooperative Self-Assembly of Discoid Dimers: Hierarchical Formation of Nanostructures with a pH Switch
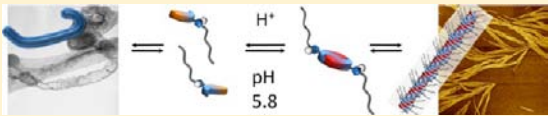
M. Tassilo Fenske,[†] Wolfgang Meyer-Zaika,[‡] Hans-Gert Korth,[†] Henning Vieker,[§] Andrey Turchanin,[§] and Carsten Schmuck*[,†]

[†]Institut für Organische Chemie, and [‡]Institut für Anorganische Chemie, Universität Duisburg-Essen, Universitätsstraße 7, 45141 Essen, Germany;

[§]Faculty of Physics, University of Bielefeld, Universitätsstraße 25, 33615 Bielefeld, Germany.

Ⓢ *Supporting Information*

ABSTRACT: Derivatives of the self-complementary 2-guanidiniocarbonyl pyrrole 5-carboxylate zwitterion (**1**) (previously reported by us to dimerize to **1•1** with an aggregation constant of ca. $>10^{10}$ M^{-1} in DMSO) aggregate in a diverse manner depending on, e.g., variation of concentration or its protonation state. The mode of aggregation was analyzed by spectroscopic (NMR, UV) and microscopic (AFM, SEM, HIM, and TEM) methods. Aggregation of dimers of these zwitterions to higher supramolecular structures was achieved by introduction of *sec*-amide substituents at the 3-position, i.e., at the rearward periphery of the parent binding motif. A butyl amide substituent as in **2b** enables the discoid dimers to further aggregate into one-dimensional (rod-like) stacks. Quantitative UV dilution studies showed that this aggregation is strongly cooperative following a nucleation elongation mechanism. The amide hydrogen seems to be essential for this rod-like aggregation, as neither **1** nor a corresponding *tert*-amide congener **2a** form comparable structures. Therefore, a hydrogen bond-assisted $\pi-\pi$-interaction of the dimeric zwitterions is suggested to promote this aggregation mode, which is further affected by the nature of the amide substituent (e.g., steric demand), enabling the formation of bundles of strands or even two-dimensional sheets. By exploiting the zwitterionic nature of the aggregating discoid dimers, a reversible pH switch was realized: dimerization of all compounds is suppressed by protonation of the carboxylate moiety, converting the zwitterions into typical cationic amphiphiles. Accordingly, typical nanostructures like vesicles, tubes, and flat sheets are formed reversibly under acidic conditions, which reassemble into the original rod-like aggregates upon readjustment to neutral pH.

INTRODUCTION

Whereas the self-assembly of polymer-based materials is well established, the controlled self-assembly of small, nonpolymeric building blocks into well-defined larger nanostructures is still an emerging area of research, especially for self-assembly in polar solution. In recent years, progress has been made using, for example, the stacking of aromatic amphiphiles,[1,2] aggregation of metallo-supramolecular structures,[3,4] or electrostatically driven self-assembly of organic ions.[5,6] It is even more interesting—but also more challenging—to find self-assembling systems which allow for switching back and forth between different types of nanostructures using an external stimulus[7] such as temperature,[8,9] metal ions,[10,11] light,[12,13] pH,[14−16] or solvent.[17,18] Obviously, in the latter case switching back and forth between different nanostructures is not really possible without further ado. We now report that the small self-complementary zwitterions **2(b−e)** and **3** (Scheme 1) can hierarchically self-assemble in polar solution (DMSO) first into planar dimers, which then further aggregate in a cooperative manner into rigid nanofibers or flat sheets, depending on the packing parameter of the monomers. These higher aggregates result from π-stacking of the discoid dimers formed by the self-complementary zwitterions. Therefore, the aggregation mode can be controlled by changing the protonation state of the zwitterions. Protonation leads to cationic amphiphiles which
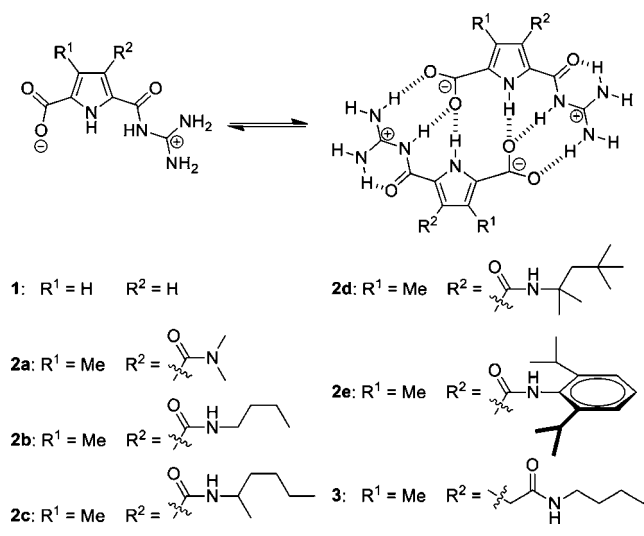
form classical nanostructures such as vesicles or tubes instead of rods.

Ten years ago we reported that 2-guanidiniocarbonyl pyrrole 3-carboxylate zwitterion **1** forms very stable ion-paired dimers **1•1** (Scheme 1) even in polar solution ($K > 10^{10}$ M^{-1} in DMSO; $K > 10^2$ M^{-1} in water, respectively).[19,20] However, this zwitterion did not form any specific aggregates larger than dimers but precipitated even at low micromolar concentrations (DMSO). It is well-known that aromatic systems can aggregate into one-dimensional fibers when functionalized with amide groups.[21−25] These aggregates are often formed *via* intermolecular $\pi-\pi$-stacking of aromatic cores and are further stabilized by intermolecular hydrogen bonds along the periphery of such stacks. Based on these observations we envisioned that a new type of zwitterions **2(b−e)** and **3**, derived from **1** by introducing a *sec*-amide group in the 3-position of the pyrrole, will also form dimers, which could then further aggregate into rod-like nanostructures in a comparable manner as reported for planar aromatic discoid molecules. In this case, however, the individual planar aromatic stacking units would be the result of a self-assembly processes themselves. For characterization of the resulting aggregates, and to elucidate the mechanism

Scheme 1. Molecular Structure of Self-Complementary Zwitterions 1, 2(a−e), and 3 and Their Corresponding Dimers

1: R^1 = H   R^2 = H

2a: R^1 = Me   R^2 =

2b: R^1 = Me   R^2 =

2c: R^1 = Me   R^2 =

2d: R^1 = Me   R^2 =

2e: R^1 = Me   R^2 =

3: R^1 = Me   R^2 =

underlying their formation, concentration-dependent UV/vis measurements, atomic force microscopy (AFM), helium ion microscopy (HIM), and scanning, as well as transmission electron microscopy (SEM, TEM) were employed.

■ RESULTS AND DISCUSSION

Microscopic Studies of Aggregates Based on 2(a−c). The first concrete evidence for the formation of larger aggregates than just dimers came from AFM-, SEM-, and TEM-studies. Images obtained from 1 mM solutions of butyl amide **2b** and 2-hexylamide **2c** clearly showed one-dimensional aggregates (Figure 1) with a length of several hundred nanometers. The fibers are rather straight, thus indicating a
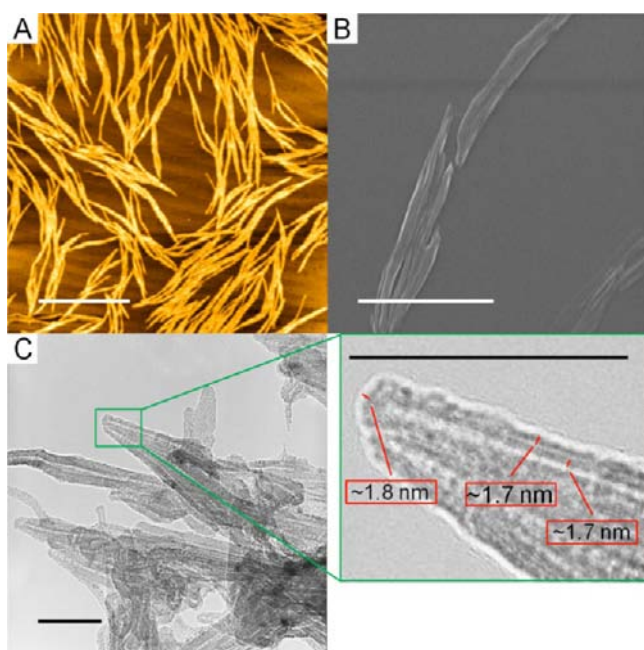

Figure 1. AFM- (A), SEM- (B), and TEM-images (C) of 1.0 mM solutions (DMSO) of zwitterions **2b** (A, B) and **2c** (C) (Scale bar: A = 2 μm; B = 1 μm; C = 50 nm; z-scale A = 1.4 nm).

certain stiffness. Interestingly, the *sec*-amide **2a**, which does not have an amide NH in the peripheral amide group, did not form any such aggregates (see Supporting Information). Also, the parent zwitterion **1** did not form any ordered aggregates but precipitates from solution at concentrations > *ca.* 10 mM. AFM and SEM images of **2b** and **2c** (Figure 9A) revealed fibers appearing almost identically. Aggregates of both compounds are characterized by a thickness of about 40−50 nm, with some small variation in their respective height. The fibers visible in the AFM-image of butyl amide **2b** (Figure 1A) have an average height of *ca.* 1.1 ± 0.2 nm, while fibers formed by 2-hexyl amide **2c** have a height of *ca.* 1.9 ± 0.2 nm (c.f. Figure 8A and Supporting Information for corresponding height profiles), which is in agreement with the increased molecular size of **2c** compared to **2b**. Indeed, the measured heights correspond quite well to the dimensions of dimerized monomers **2b•2b** and **2c•2c**, respectively, as estimated from molecular mechanics calculations (Figure 2). These dimensions were also confirmed
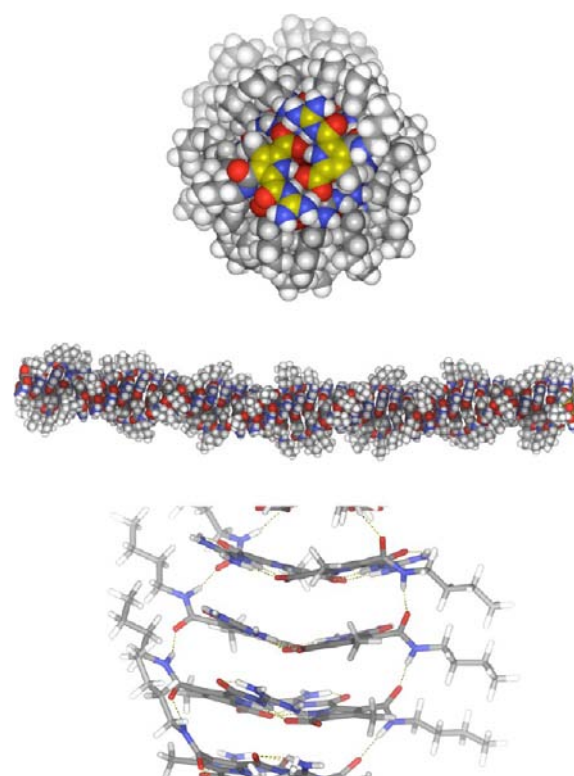

Figure 2. Calculated structure of a one-dimensional rod obtained from the stacking of discoid dimers **2b•2b** (one shown in yellow). The modeling suggests H-bonds between amide groups along the inner core of the rod.

by DOSY experiments, which delivered a hydrodynamic radius of *ca.* 1.4 nm (assuming spherical particles) for dimer **2b•2b** (10 mM solution in DMSO) in good agreement with the results from microscopic images.[26] However, as the lateral thickness of these fibers is significantly bigger than the size of the dimers, this suggests that the fibers are not individual rods (formed by π−stacking of dimerized zwitterions), but rather larger bundles resulting from further lateral aggregation of such individual rods. This could indeed be confirmed by a SEM-image of the (identical) surface generated for the AFM-experiment. It is clearly visible that these fibers are aggregates of the expected smaller rods (Figure 1B). The same was observed

in TEM-images of compound **2c**: again, it can be clearly seen that the fibers are formed from aggregates of smaller rods. The dimensions of these individual rods (1.7 ± 0.1 nm, see Figure 1C, zoom region) contained within the bigger bundles are in excellent agreement with their height obtained from the AFM-experiment and the molecular size expected for the discoid dimers of these zwitterions (see Figure 2). Based on these images, the bigger strands are likely to consist of 10−30 individual fibers.

Molecular Modeling Studies. Molecular mechanics calculations were performed to visualize the one-dimensional rods seen in the microscopic images of **2b** and to probe their molecular dimensions. A Monte Carlo conformational search (*Macromodel* v 8.5, OPLS_2005 force field with GB/SA water solvation, 50 000 steps) revealed that the planar discoid dimers, formed from the self-assembly of zwitterion **2b**, can further stack into a one-dimensional rod (Figure 2). The dimerized zwitterions form the inner core of these stacks which is coated by the butyl amide groups. The estimated overall thickness of the rod (*ca.* 1.5 nm) is in excellent agreement with the diameter of the individual rods as extracted from the TEM images.

UV-Dilution Studies. Having thereby affirmed that *sec*-amide substituted zwitterions **2b** and **2c** aggregate first into dimers and then into one-dimensional rod-like structures, we set out to investigate the concentration dependency of this aggregation process using UV/vis dilution studies. It quickly became obvious that the disassembly of aggregates based on zwitterions like **2b** only occurs at very low concentration (<0.3 mM). Consequently, NMR-dilution experiments, covering a concentration range from 40 mM to 1.5 mM, were not informative in these cases (see Supporting Information). UV-spectroscopy, being more sensitive at lower concentration, however, provided the means to monitor the disassembly process. For example, UV-spectra of *sec*-amide **2b** were measured within the concentration range of 0.33 mM and 9 nM (Figure 3). Plotting the molar absorptivity ε against the corresponding wavelengths at different concentrations reveals a bathochromic shift of the absorption maxima of about 20 nm below the concentration of 0.11 mM; with an isosbestic point at 312 nm. At concentrations below 18 nM no further changes of the molar extinction coefficients ε were observed. Due to the

high dimerization constant of the zwitterions ($K > 10^{10}$ M^{-1} in DMSO),[19,20] the changes in the UV spectra, which start already upon dilution below a concentration of 0.1 mM cannot reflect the formation of the dimers from the zwitterions but must represent the stacking of these dimers into larger aggregates. The occurrence of a clear isosbestic point further suggests a distinct and ordered structure for these larger aggregates, rather than just unspecific aggregation (as in **1**). The bathochromic shift of ca. 20 nm is then a result of the electronic changes accompanying the stacking of the discoid dimers into the rods.

For amide functionalized aromatics, it had already been shown that the formation of related one-dimensional rods from $\pi-\pi$-interactions of aromatic cores can be promoted by hydrogen bonds along the stacks.[21−25] As the amide group in our zwitterions is also crucial for the formation of the one-dimensional aggregates it is most likely that H-bonds between the butyl amide groups also help stabilize the structure. Neither the parent zwitterion **1** without any amide group nor zwitterion **2a** with a dimethyl amide group, both lacking the potential to form H-bonds, showed any evidence for the formation of specific aggregates in AFM-, SEM-, and TEM-experiments. Accordingly, the changes in the UV spectrum of **2a** (Figure 4)
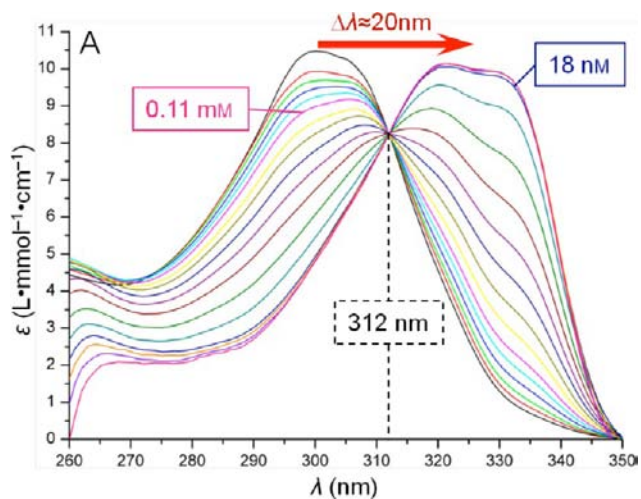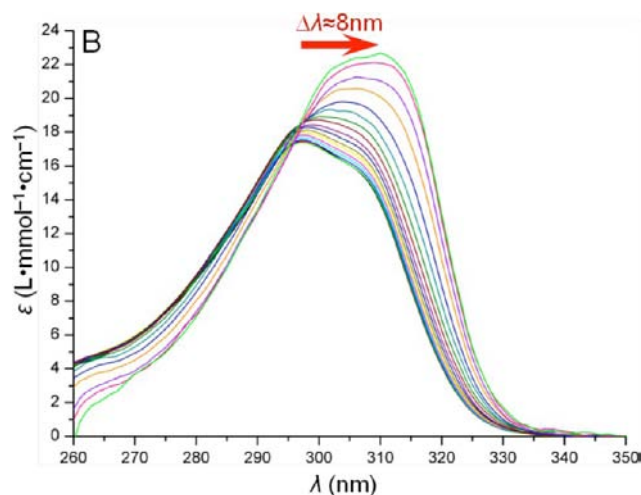

Figure 4. Concentration dependent UV/vis absorption spectra of **2a** (0.33 mM to 4 nM in DMSO). Arrow indicates the direction of change with decreasing concentration.

are completely different from those for **2b**. Upon dilution from 0.16 mM to 4 nM a slight increase of the molar extinction coefficients ε was observed, but no isosbestic point and only a small bathochromic shift of about 8 nm were detected. In contrast, all other zwitterions (**2c−e**, **3**) which again have an amide NH show similar UV changes as **2b** (see Supporting Information) and also formed ordered aggregates as seen in the corresponding microscopic images (Figure 9). Therefore, one can conclude that the formation of the one-dimensional rods which are visible in the AFM-, SEM-, and TEM-experiments for **2b** is favored by H-bonds along the side of the stack as observed for other amide functionalized aromatics. However, the important difference here is that the aggregating disc itself is already the result of a self-assembly process, namely, the dimerization of the zwitterion.

The molecular mechanics calculations also suggested such stabilizing H-bonds between the amide groups of the stacked dimers (Figure 2). For the formation of these H-bonds, however, the amide group has to rotate out of the plane of the

Figure 3. Concentration dependent UV/vis absorption spectra of **2b** (0.33 mM to 9 nM in DMSO). Arrow indicates the direction of change with decreasing concentration.

dimers, so that the carbonyl-oxygen and the amide-NH point toward the corresponding amide groups of an associated disc above or below, respectively. This rotation changes the electronic properties of the dimers and together with the π-stacking is hence most likely responsible for the observed hypsochromic shift in the UV spectra which occurs during rod-formation. To test this, we simulated the consequences of such a rotation by time dependent DFT calculations (PBE0/6-31G(d) level, PCM method with DMSO as solvent) of the two conformers **A** and **B** of model compound **4** (Figure 5).
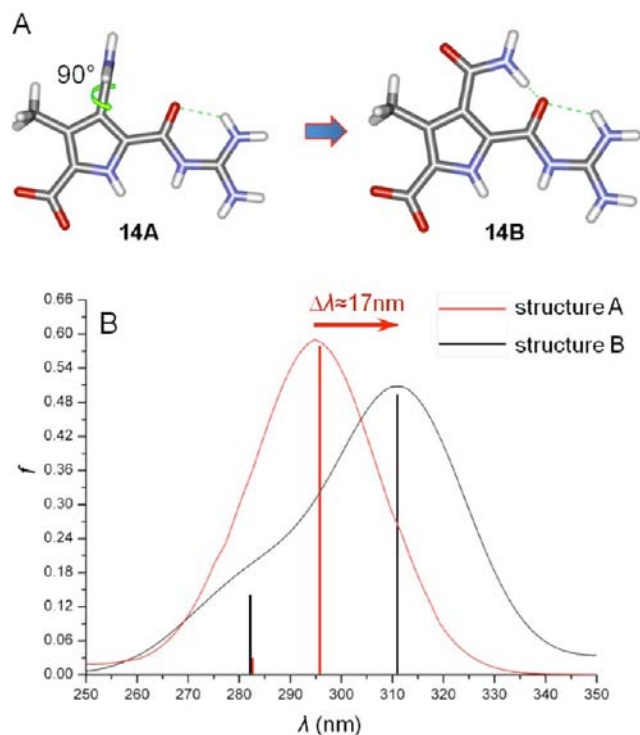

Figure 5. TD-DFT computed UV-spectra of the two conformers **A** and **B** of model compound **4**. Depicted as lines are the oscillation strengths (f) for both conformers. For the visualization of the UV-spectra Gauss functions with a half width of $\Delta\lambda/2 = 15$ were used.

Conformers **4A** and **4B** differ only in the orientation of their peripheral amide bond. While this functional group is oriented 90° perpendicular to the plane of the zwitterion within structure **4A** (as a model for its orientation in the aggregated stacks) it is parallel in **4B** (as in the nonstacked dimers). Using time dependent DFT calculations the influence of these two possible orientations of the amide group onto the electronic structure of the zwitterion was estimated. A shift of the UV-maxima of 17 nm was calculated if the amide bond is rotated from the perpendicular (**4A**) to the parallel orientation (**4B**). This shift is in excellent agreement with the bathochromic shift observed upon dilution and hence deaggregation of the dimers of **2b**. Therefore, a similar change in the orientation of the amide group seems to occur during rod-formation.

Next to the structural effects discussed above, the mechanism of aggregation can be deduced from a quantitative analysis of the UV-dilution experiments.[27] For this analysis the degree of aggregation α was plotted against the corresponding concentrations (Figure 6). As evident from the UV spectra of compound **2b** (Figure 3) the molar absorptivity does not change anymore upon dilution below 4 nM. This indicates that the aggregates responsible for the UV changes are completely
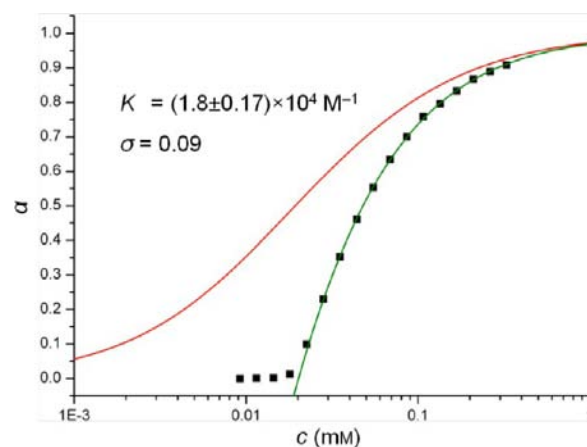

Figure 6. Plotting the degree of aggregation α of **2b** against the concentration (black squares). The data can only be fitted to a strongly cooperative aggregation mode (green) but clearly not to an isodesmic growth model (red).

disassembled at this (and lower) concentrations. Hence the molar absorptivity at this concentration corresponds to the unstacked dimers ($\alpha = 0$). The molar absorptivity of the fully aggregated species ($\alpha = 1$) can be obtained from an extrapolation of the spectral changes at higher concentration (see Supporting Information for more details). With these two values for the molar absorptivities of the unstacked dimers and the aggregated rods the degree of aggregation for each concentration can be easily calculated. As shown in Figure 6, the degree of aggregation α does not increase smoothly. Aggregation only occurs above a critical concentration of ca. 15 μM. This behavior is typical for a cooperative nucleation elongation mechanism. Aggregation first requires the initial formation of a small nucleus. Once this nucleus (often a dimer, i.e., in this case a tetramer formed of two discoid dimers of type **2•2**) is formed, above the critical concentration (which depends on the association constant K_2 for the formation of this nucleus), rapid aggregation occurs because the subsequent elongation steps (which are characterized by an association constant K) are energetically more favorable than the initial formation of the nucleus ($K > K_2$). The alternative to such a cooperative aggregation would be the so-called isodesmic growth, in which each aggregation step from monomer to dimer to any larger aggregate is characterized by the same association constant K. It is clearly evident that aggregation of **2b** is not an isodesmic process (red line in Figure 6)[23,28] but a strongly cooperative one. The cooperative nucleation elongation model (also called K_2/K-model) can be quantitatively described with the following equation:[28]

$$\varepsilon(c) = \frac{2Kc + \sigma - \sqrt{4Kc + \sigma^2}}{2K^2c^2}(\varepsilon_f - \varepsilon_a) + \varepsilon_a$$

ε denotes the measured molar absorptivity at each concentration; ε_f and ε_a are the values for the free and the aggregated species; K is the binding constant, σ is the degree of cooperativity (K_2/K), and c is the total compound concentration in the sample. The data fitting (green line in Figure 6) provides an association constant of $K = 1.8 \times 10^4$ M^{-1} for the stacking of the dimeric discs into the rods and a degree of cooperativity of $\sigma = 0.09$, indicating that this is indeed a highly cooperative process.

Is the cooperative nucleation elongation mechanism compatible with the formation of π-stacked rods from discoid dimers as discussed so far? As deduced from the UV spectral changes (Figure 4) aggregation requires the rotation of the amide group out of planarity. At least for the two model conformers **4A** and **4B** the energy difference between these two orientations is *ca.* 15 kcal/mol. For the stacking of the first two planar discoid dimers to form a nucleus four amide groups have to be rotated out of planarity. Hence, this energy penalty has to be paid four times. For any subsequent stacking of the next discoid dimer onto an already existing nucleus or any larger aggregate, only two amide groups have to be rotated. Consequently, the formation of the nucleus is expected to be less favorable than the subsequent elongation step. Already based on this simple model, a cooperative aggregation is expected and reasonable.

The aggregation mechanism of compound **2b** can therefore be described as shown in Figure 7. Due to the extraordinarily
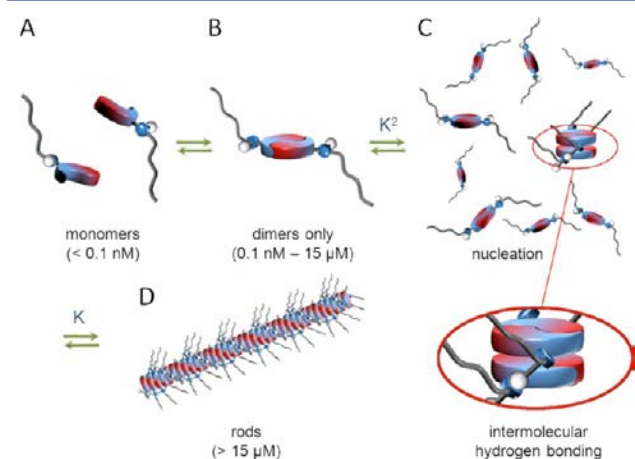

Figure 7. Schematic self-assembly of the zwitterion **2b** starting at infinite diluted solution (A) *via* dimerization (B) and nucleation (C) to formation of one-dimensional rod-like structures (D).

high association constant of the zwitterionic binding motif **1** ($K > 10^{10}$ M^{-1} in DMSO)[20] butyl amide **2b** exists in its monomeric state only at extreme dilution (A). Already at nanomolar concentrations, mainly dimers **2b•2b** are present (B). At a critical concentration of about 15 μM these discoid dimers start to aggregate into the first nuclei (C), which then on further increase of the concentration readily grow in a strongly cooperative manner into one-dimensional rods (D).

A similar cooperative growth was found for all other zwitterions **2(c–e)** and **3** with an amide NH group. The corresponding aggregation constant K and the degree of cooperativity σ as obtained from the respective UV-dilution experiments (see Supporting Information) are summarized in Table 1. It can be seen that the nature of the amide substituents has an effect on the association constant and hence the stability of the larger aggregates. The structural difference between **2b** and **2c** is only small, which is reflected in their respective and nearly identical aggregation constants. The larger *tert*-octyl side chain of **2d**, however, leads to a 30 times larger aggregation constant. This increase most likely reflects enhanced van der Waals interactions between the larger alkyl side chains along the core of the π-stacked dimers. An even larger aggregation constant is obtained for the diisopropylphenyl amide **2e**. This increased stability points toward additional π−π-interactions

Table 1. Calculated Aggregation Constant K and Degree of Cooperativity σ for the Aggregation of Dimers Based on Zwitterions 2(b-e) and 3 into Rods[a]

	R^2 (cf. scheme 2)	K in M^{-1}	σ
2b		$(1.8\pm0.17) \cdot 10^4$	0.09
2c		$(3.0\pm0.62) \cdot 10^4$	0.05
2d		$(5.6\pm4.0) \cdot 10^5$	0.01
2e		$(7.8\pm1.0) \cdot 10^5$	0.007
3		$(3.5\pm1.3) \cdot 10^4$	0.12

[a]The data are obtained from the corresponding UV dilution studies.

between the peripheral aromatic moieties. The aggregation constants of butyl amide **2b** and its homo congener **3** are again very similar. A similar tendency is observed for the degrees of cooperativity σ. The values for **2b−c** and **3** are nearly identical, whereas for **2d** and **2e** the degree of cooperativity increases significantly.

Microscopic Studies of Aggregates Based on 2(c−e) and 3. To further determine the structural influence of the peripheral amide substituent onto the mode of aggregation, additional AFM-images of zwitterions **2(c-e)** and **3** were taken. For zwitterion **2c** (Figure 8A) identical rod-like aggregates as for **2b** (Figure 1) are observed which is hardly surprising given the structural similarity of both zwitterions. The larger *tert*-octyl amide **2d** (Figure 8B), showed a much stronger tendency for lateral aggregation of the rods into larger bundles. In the AFM-image large areas covered with strongly aggregated, almost layer-like structures with an average height of 1.8 ± 0.2 nm are seen. The 2,6-diisopropyl-phenyl amide **2e** produced only layer-like structures (Figure 8C). In this case most of the surface was covered with a layer of an average thickness of 1.5 ± 0.2 nm. Again, the height of this layer fits very well with the estimated size of the discoid dimers **2e•2e**.

The AFM-image of homo amide **3** (Figure 8D) exclusively shows circular layer-like structures with a height of about 2.0 ± 0.2 nm, which again correlates to the dimensions calculated for the dimerized zwitterion **3•3**. Such pronounced layer-like aggregation was somehow unexpected with respect to its structural similartity to **2b**, which readily produced fiber-like bundles of rods (see above). Somehow the rods formed by homo amide **3** seem to be more prone to lateral aggregation than in the case of **2b**. To further investigate the aggregation of **3**, SEM-, HIM-, and TEM-images were recorded (Figure 9).
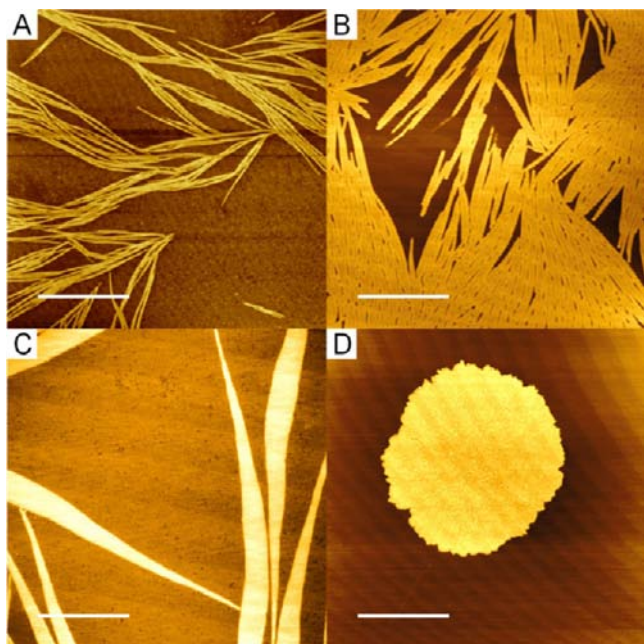
Figure 8. AFM-images of 1.0 mM solutions of the zwitterions **2c** (A), **2d** (B), **2e** (C), and **3** (D). (Scale bar: 2 mm; z-scale A = 3.9 nm, B = 3.9 nm, C = 2.7 nm, D = 3.0 nm.)
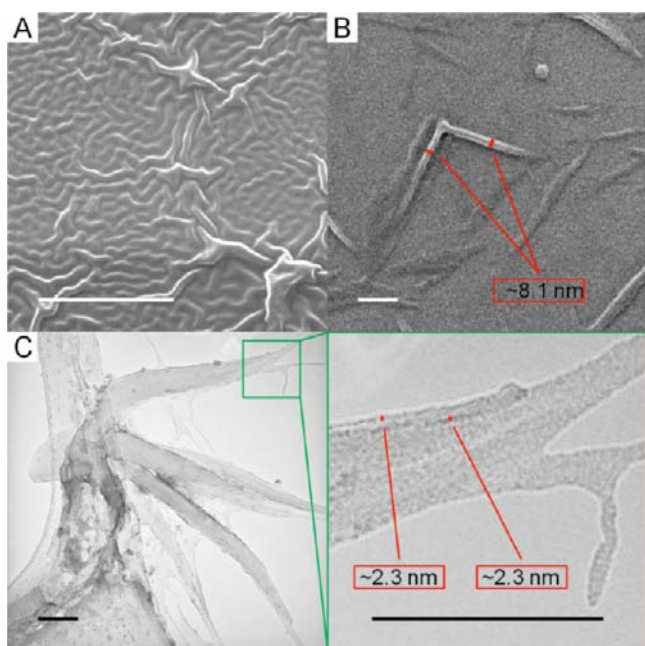

Figure 9. SEM- (A), HIM- (B), and TEM-images (C) of 1 mM solutions of zwitterion **3**. (Scale bar: A = 1 μm; B = 50 nm; C = 100 nm.)

The existence of a layer-like structure was confirmed in all three cases. SEM-images showed a foil-like material that appeared to be shrunken due to sample preparation, as coating the sample with carbon required heating. HIM- and TEM-images, however, also show the expected linear aggregates besides layer structures. In both cases, the linear aggregates seemed to be embedded into the sheet-like structure. The dimensions of around 8 nm estimated from the HIM-image (Figure 9B) suggested that these linear aggregates are bundles resulting from lateral aggregation of individual rods. TEM-images were

able to resolve these individual rods, the width of which (2.3 nm, see Figure 9C and zoom region) corresponds again quite well to the size of the dimerized zwitterion **3·3**. Hence, despite the overall different appearance of the AFM images of **3**, its aggregation mode seems to be identical to that of the other zwitterions. Obviously, the main difference is that the lateral aggregation of the individual rods and the fiber-like bundles is more pronounced. Hence, homoamide **3** has a stronger inclination to form two-dimensional aggregates (upon evaporation of the solvent on a mica surface) than **2b**.

In conclusion, the different tendency of the zwitterions to form two-dimensional aggregates, as seen in the AFM-images (Figure 8A→D), depends on their possibility for lateral interactions between the rods. The alkyl amides **2b**, **2c**, and **2d** can interact laterally only by van der Waals forces and therefore have only a weak tendency to form two-dimensional aggregates. Accordingly, in the AFM images mainly linear structures are seen. The 2,6-diisopropylphenyl amide **2e** can most likely form additional $\pi-\pi$-interactions to neighboring strands, which increases the tendency toward two-dimensional aggregation. Finally, homo amide **3**, which might also form lateral hydrogen bonds as well, appears only as a 2D-layer in the AFM-image.

Studies on Switching the Aggregation Mode by Protonation. The ability to influence supramolecular aggregation by varying an external factor (e.g., pH) in a *reversible* manner is of pivotal interest. As recognized before, the aggregation of the zwitterionic binding motif **1** can be directly affected by changing its protonation state.[19] Only the zwitterion can form dimers; neither the protonated nor the deprotonated forms obtained after addition of either acid or base are self-complementary. Therefore, supramolecular structures formed by the dimers of zwitterions of type **2** should be sensitive to changes in their protonation state as well, and a drastic change in their aggregation mode and the morphologies of the resulting structures should occur. Attempts to investigate such a morphology switch by deprotonation failed, since the addition of base to a DMSO solution of zwitterions **2(b–e)** only resulted in complete precipitation. Obviously the anionic compounds are not soluble enough to study their aggregation in DMSO. However, addition of aqueous HCl (1 M, 10 equiv) to the respective zwitterions in DMSO produced a homogeneous solution, in which complete protonation of the zwitterions was confirmed by ^{1}H NMR.

Again, AFM and TEM were employed to investigate the supramolecular structures formed by the protonated compounds **2b•H⁺–2e•H⁺**. To our delight a drastic change in morphology was indeed observed after protonation. For example, as discussed above, AFM-images recorded from butyl amide **2b** (Figure 10A, also see Figure 1) revealed rods formed by linear aggregation of dimers **2b•2b**. In contrast, the protonated form **2b•H⁺** produced solvent filled vesicles (Figure 10B). These vesicles have a height of *ca.* 3–4 nm and a size of *ca.* 50 nm. Given a certain softness of these structures in the AFM experiment, this height corresponds to a classical bimolecular layer structure of the vesicles. As **2b•H⁺** resembles classical cationic amphiphiles the formation of such vesicular structures is reasonable. After readjustment of the original protonation state (**2b•H⁺→2b**) by addition of an equal amount of base (aq. NaOH), the original rods of stacked discoid dimers **2b•2b** are formed again (Figure 10 C). All other zwitterions behave in a similar way. Figure 11 shows AFM- and SEM-images for **2c•H⁺–2e•H⁺** (for **3•H⁺** see Supporting
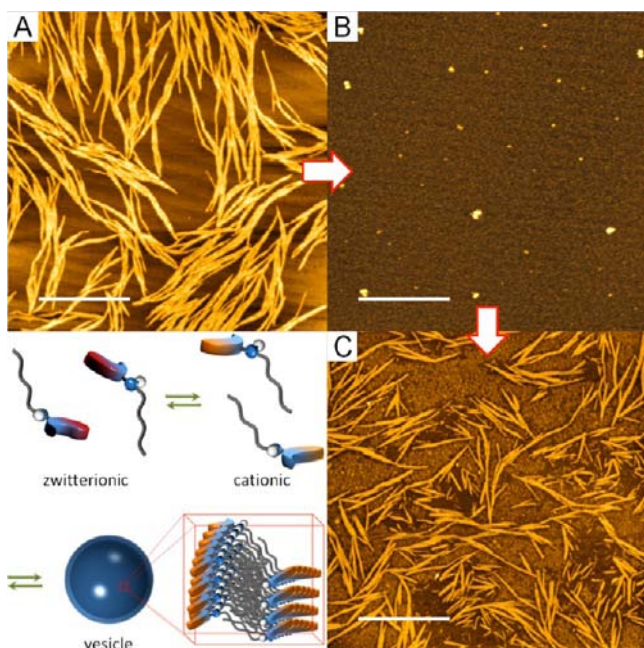
Figure 10. Switching the morphology of aggregates of **2b** by reversible protonation and deprotonation (1.0 mm, DMSO): (A) AFM image of zwitterion **2b**; (B) Protonated version **2b•H**⁺ after the addition of 10 equiv of HCl; (C) Reformation of the zwitterion **2b** after the addition of the same amount of NaOH to the solution of B. Precipitated NaCl can be seen between the supramolecular rods. Scale bar = 2 μm; z-scale: A = 1.4 nm, B = 6.6 nm, C = 3.6 nm.

Information). While only small differences in the aggregation of dimers formed by butyl amide **2b** and 2-hexyl amide **2c** were detected (Figures 1A and 8A), more pronounced differences were visible in the aggregates formed by their protonated congeners **2b•H**⁺ and **2c•H**⁺. Only vesicular and therefore spherical particles are formed from a 10 mM solution of protonated butyl amide **2b•H**⁺ in DMSO (Figure 11A). From an equivalent solution of protonate 2-hexyl amide **2c•H**⁺, tube-like structures emerged in addition to vesicles with an average height of 3.3 ± 0.2 nm (Figure 11B). As these tube-like structures have the same diameter as the vesicles, it could not be excluded from the AFM image that these structure are simply clusters of individual vesicles. However, TEM-images of **2c•H**⁺, like the one depicted in Figure 11C, clearly showed that the described structures are indeed hollow tubes. As shown in the zoom-region, even fused multilayer substructures are visible. Therefore, it appears that these nanotubes originate from the fusion of individual vesicles.

Whereas **2b•H**⁺ and **2c•H**⁺ formed vesicles or tubes, **2d•H**⁺ and **2e•H**⁺ produced flat layered aggregates in a concentration dependent manner (c.f. Supporting Information). AFM images of **2d•H**⁺ (Figure 11D) and **2e•H**⁺ (Figure 11E) obtained from 1 mM solutions show structures with an average height of 1.5 ± 0.2 nm and 1.4 ± 0.2 nm, respectively. The surface density of these layer-like structures is much higher in the case of diisopropylphenyl amide **2e•H**⁺, with some additional precipitated material also present. The height of these flat structures corresponds to the molecular dimension of *ca.* 1.3 to 1.6 nm for **2d•H**⁺ and **2e•H**⁺ (as suggested by molecular modeling). Obviously **2d•H**⁺ and **2e•H**⁺, which have a more cylindrical shape than **2b•H**⁺ and **2c•H**⁺ due to the larger size of their corresponding side chains, not only form bigger vesicles,[29,30] but these vesicles then tend to collapse on the
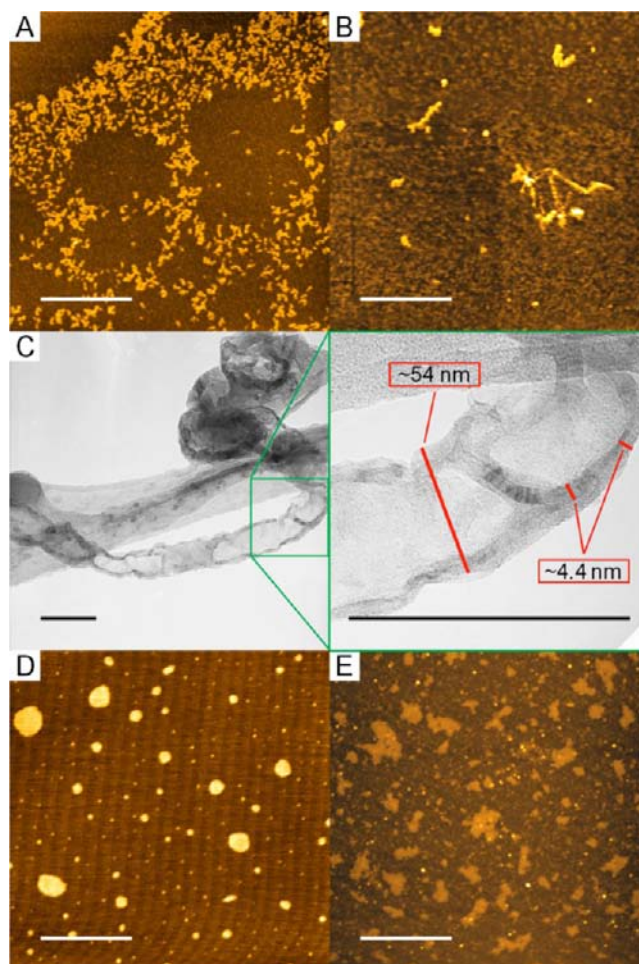

Figure 11. AFM (A, B) and TEM-images (C) of a 10 mM solution of the protonated versions of **2b•H**⁺ (A), **2c•H**⁺ (B, C), and AFM (D,E) images of a 1 mM solution of **2d•H**⁺ (D) and **2e•H**⁺ (E). (Scale bar: A, B, D, E = 2 mm; C = 100 nm; z-scale A = 6.8 nm, B = 6.5 nm, C = 2.7 nm, D = 2.6 nm, E = 7.4 nm.)

surface forming flat monolayers.[31,32] Therefore, the data shown here clearly demonstrates that self-complementary zwitterions of type **2** allow for reversible morphology switching of the resulting aggregates. Simply by reversible protonation and deprotonation fiber-like structures can be transformed into vesicles and tubes and *vice versa*.

■ CONCLUSION

We were able to show here that zwitterions of type **2** aggregate hierarchically, first into discoid dimers, which then further assemble into rods based on π−π-stacking. The formation of rods by π-stacking of aromatic amides is well-known; in this case, however, the stacking unit itself is already the result of a self-assembly process, namely, the dimerization of the zwitterions. Recently, two examples of similar hierarchical rod formation, based on dimeric, and indeed trimeric, discoid aggregates based on H-bonding, have been reported by Meijer[33] and Hud,[34] respectively. However, as the structures described within this paper are based on ionic interactions within the discoid dimers, strongly cooperative π-stacking of these dimers into rods following a nucleation elongation mechanism was now also achieved in polar solvents (DMSO). Depending on the size and nature of the amide side chains, the tendency of the rods to form bigger bundles increases from

molecule **2b** to **2e**. As the discoid dimers are essential for rod formation, the self-assembly mode can be completely changed by protonation of the zwitterions. Hence, zwitterions **2** are converted into classical cationic amphiphiles **2•H⁺** which form vesicles, tubes, and flat sheets, instead of linear rods. Such switchable nanomaterials might be of interest for further development of functional materials.

■ ASSOCIATED CONTENT

Ⓢ Supporting Information

Detailed synthetic procedures and spectroscopic characterization for all new compounds, as well as detailed description of molecular modeling calculations, UV/vis titration, and microscopic imaging experiments. This material is available free of charge via the Internet at http://pubs.acs.org.

■ AUTHOR INFORMATION

Corresponding Author
*E-mail: carsten.schmuck@uni-due.de.
Notes
The authors declare no competing financial interest.

■ ACKNOWLEDGMENTS

■ REFERENCES

(1) Bae, J.; Choi, J. H.; Yoo, Y. S.; Oh, N. K.; Kim, B. S.; Lee, M. *J. Am. Chem. Soc.* **2005**, *127*, 9668−9669.

(2) Fernández, G.; García, F.; Aparicio, F.; Matesanz, E.; Sánchez, L. *Chem. Commun.* **2009**, 7155−7157.

(3) Lützen, A.; Hapke, M.; Griep-Raming, J.; Haase, D.; Saak, W. *Angew. Chem., Int. Ed.* **2002**, *41*, 2086−2089.

(4) Frischmann, P. D.; Guieu, S.; Tabeshi, R.; MacLachlan, M. J. *J. Am. Chem. Soc.* **2010**, *132*, 7668−7675.

(5) Tanaka, Y.; Katagiri, H.; Furusho, Y.; Yashima, E. *Angew. Chem., Int. Ed.* **2005**, *117*, 3935−3938.

(6) Schmuck, C.; Rehm, T.; Klein, K.; Gröhn, F. *Angew. Chem., Int. Ed.* **2007**, *46*, 1693−1697.

(7) Fenske, T.; Korth, H. G.; Mohr, A.; Schmuck, C. *Chem.—Eur. J.* **2012**, *18*, 738−755.

(8) García, F.; Aparicio, F.; Marenchino, M.; Campos-Olivas, R.; Sánchez, L. *Org. Lett.* **2010**, *12*, 4264−4267.

(9) Nieuwenhuizen, M. M. L.; de Greef, T. F. A.; van der Bruggen, R. L. J.; Paulusse, J. M. J.; Appel, W. P. J.; Smulders, M. M. J.; Sijbesma, R. P.; Meijer, E. W. *Chem.—Eur. J.* **2010**, *16*, 1601−1612.

(10) Hui, J. K.-H.; MacLachlan, M. J. *Dalton Trans.* **2010**, *39*, 7310−7319.

(11) Golubkov, G.; Weissman, H.; Shirman, E.; Wolf, S. G.; Pinkas, I.; Rybtchinski, B. *Angew. Chem., Int. Ed.* **2009**, *48*, 926−930.

(12) Kanaya, A.; Takashima, Y.; Harada, A. *J. Org. Chem.* **2011**, *76*, 492−499.

(13) Wang, Y.; Han, P.; Xu, H.; Wang, Z.; Zhang, X.; Kabanov, A. V. *Langmuir* **2010**, *26*, 709−715.

(14) Dong, S.; Luo, Y.; Yan, X.; Zheng, B.; Ding, X.; Yu, Y.; Ma, Z.; Zhao, Q.; Huang, F. *Angew. Chem., Int. Ed.* **2011**, *50*, 1905−1909.

(15) Rodler, F.; Linders, J.; Fenske, T.; Rehm, T.; Mayer, C.; Schmuck, C. *Angew. Chem., Int. Ed.* **2010**, *49*, 8747−8750.

(16) Voskuhl, J.; Fenske, T.; Stuart, M. C. A.; Wibbeling, B.; Schmuck, C.; Ravoo, B. J. *Chem.—Eur. J.* **2010**, *16*, 8300−8306.

(17) Hill, J. P.; Jin, W.; Kosaka, A.; Fukushima, T.; Ichihara, H.; Shimomura, T.; Ito, K.; Hashizume, T.; Ishii, N.; Aida, T. *Science* **2004**, *304*, 1481−1483.

(18) Fernández, G.; García, F.; Sánchez, L. *Chem. Commun.* **2008**, 6567−6569.

(19) Schmuck, C. *Eur. J. Org. Chem.* **1999**, 2397−2403.

(20) Schmuck, C.; Wienand, W. *J. Am. Chem. Soc.* **2003**, 452−459.

(21) Nguyen, T. Q.; Martel, R.; Avouris, P.; Bushey, M. L.; Brus, L.; Nuckolls, C. *J. Am. Chem. Soc.* **2004**, *126*, 5234−5242.

(22) Nguyen, T.-Q.; Martel, R.; Bushey, M.; Avouris, P.; Carlsen, A.; Nuckolls, C.; Brus, L. *Phys. Chem. Chem. Phys.* **2007**, *9*, 1515−1532.

(23) Smulders, M. M. J.; Nieuwenhuizen, M. M. L.; de Greef, T. F. A.; van der Schoot, P.; Schenning, A. P. H. J.; Meijer, E. W. *Chem.—Eur. J.* **2010**, *16*, 362−367.

(24) Aparicio, F.; Vicente, F.; Sánchez, L. *Chem. Commun.* **2010**, *46*, 8356−8358.

(25) Nieuwenhuizen, M. M. L.; de Greef, T. F. A.; van der Bruggen, R. L. J.; Paulusse, J. M. J.; Appel, W. P. J.; Smulders, M. M. J.; Sijbesma, R. P.; Meijer, E. W. *Chem.—Eur. J.* **2010**, *16*, 1601−1612.

(26) Note that DOSY experiments do not only measure the radius of the molecule/aggregate, but rather the (larger) radius of the solvation sphere. Hence dimensions measured by DOSY are normally a bit larger than the size of the molecule itself.

(27) De Greef, T. F. A.; Smulders, M. M. J.; Wolffs, M.; Schenning, A. P. H. J.; Sijbesma, R. P.; Meijer, E. W. *Chem. Rev.* **2009**, *109*, 5687−5754.

(28) Würthner, F.; Thalacker, C.; Diele, S.; Tschierske, C. *Chem.—Eur. J.* **2001**, *7*, 2245−2253.

(29) Dörfler, H.-D. *Grenzflächen- und Kolloidchemie*; 1. Aufl.; VCH: Weinheim, 1994.

(30) Holmberg, K.; Jönsson, B.; Kronberg, B.; Lindman, B. *Surfactants and Polymers in Aqueous Solution*, 2nd ed.; John Wiley & Sons: Chichester, U.K, 2003.

(31) Ravoo, B. J.; Darcy, R. *Angew. Chem., Int. Ed.* **2000**, *39*, 4324−4326.

(32) Voskuhl, J.; Fenske, T.; Stuart, M. C. A.; Wibbeling, B.; Schmuck, C.; Ravoo, B. J. *Chem.—Eur. J.* **2010**, *16*, 8300−8306.

(33) George, S. J.; de Bruijn, R.; Tomović, Ž.; Van Averbeke, B.; Beljonne, D.; Lazzaroni, R.; Schenning, A.; Meijer, E. W. *J. Am. Chem. Soc.* **2012**, *134*, 17789−17796.

(34) Cafferty, B. J.; Gállego, I.; Chen, M. C.; Farley, K. I.; Eritja, R.; Hud, N. V. *J. Am. Chem. Soc.* **2013**, *135*, 2447−2450.